RSC Advances

PAPER

View Article Online
View Journal | View Issue

Cite this: *RSC Adv.*, 2026, **16**, 13585

Effect of primary-secondary synergistic system on the aging resistance of *Salix psammophila*/polylactic acid composites

Jianpeng Hu,*[ab] Guanlin Song,[a] Xiaomin Zhang[a] and Xin Wang[ab]

To enhance the hydrothermal aging resistance of *Salix psammophila* wood flour/polylactic acid (PLA) composites, a primary–secondary synergistic anti-aging system was constructed using antioxidant 1010 as the primary antioxidant and distearyl thiodipropionate (DSTP) as the auxiliary antioxidant, with maleic anhydride as an interfacial compatibilizer. The composites were fabricated by hot-pressing, and the effects of the synergistic system on mechanical performance and hydrothermal aging behavior were investigated. Static mechanical results showed that the 1010/DSTP system enhanced the initial mechanical properties and effectively mitigated mechanical degradation after aging. After hydrothermal aging (60 °C, 96 h), the synergistically modified composite (WPC-1/D) retained 47.38% of its flexural strength, representing a 56.54% increase compared to the aged, unmodified control. Stress–strain behavior indicated improved deformation coordination and delayed damage evolution, suggesting enhanced interfacial stability under hydrothermal conditions. Dynamic mechanical analysis further confirmed the synergistic effect, as WPC-1/D exhibited a high storage modulus of 1295.43 MPa in the glassy region after aging, together with increased loss modulus and loss factor peaks, reflecting restricted molecular chain mobility and enhanced energy dissipation. A static-dynamic mechanical correlation model was established to quantitatively describe the relationship between macroscopic mechanical degradation and viscoelastic response during hydrothermal aging. Microscopic observations revealed a multi-scale progressive aging process from damage initiation to damage penetration, clarifying the aging damage pathways. Chemical analysis showed that the O–H absorption peak of WPC-1/D shifted most slowly from 3332 cm^{-1} to 3422 cm^{-1}, the ester C=O group exhibited only slight displacement, and no new CH_3-related absorption peaks emerged; meanwhile, the carbon content increased from 73.88% to 80.03% and the oxygen content decreased from 25.92% to 18.80%, indicating suppressed hydrolysis–oxidation degradation. This study elucidates the anti-aging mechanism of the primary–secondary synergistic system and provides empirical insights and experimental evidence for improving the durability of fully biodegradable composites.

Received 19th January 2026
Accepted 2nd March 2026

DOI: 10.1039/d6ra00471g

rsc.li/rsc-advances

1 Introduction

In recent years, plant fiber-reinforced polymer composites have attracted considerable attention in the field of sustainable materials owing to their excellent mechanical properties, economic viability, and environmental friendliness.[1,2] *Salix psammophila* wood flour-reinforced polylactic acid (PLA) composites combine full biodegradability with good mechanical properties, representing an effective strategy to combat "white pollution".[3] As a dominant desert shrub in Inner Mongolia, *Salix psammophila* is characterized by high cellulose content, suitable aspect ratio, and ease of modification. Its three-dimensional network structure can effectively address the deficiencies of PLA, such as high brittleness and low impact strength.[4] Moreover, the cost of *Salix psammophila* wood flour is only 1/5–1/10 that of PLA, which can significantly reduce material costs and carbon footprint while achieving both economic and environmental benefits.

However, during long-term service, composites face aging challenges induced by environmental factors such as heat, humidity, and oxygen. The synergistic action of these factors can cause photooxidative degradation of the matrix, hydrolytic chain scission, and fiber structure disruption,[5] leading to interfacial failure and macroscopic performance decay, which severely limits their service life.[6] Although modifications and process optimizations can improve material properties to some extent,[7] aging issues remain a key constraint to their applications. Therefore, an in-depth exploration of the mechanical

[a]*College of Material Science and Art Design, Inner Mongolia Agricultural University, Hohhot 010018, China. E-mail: jianpeng0101@126.com*

[b]*Inner Mongolia Autonomous Region Key Laboratory of Sandy Shrubs Fibrosis and Energy Development and Utilization, Hohhot 010018, China*

decay and interfacial failure mechanisms of composites during aging is of great significance for improving their weatherability.

Currently, the incorporation of antioxidant 1010 or composite systems is a common anti-aging approach. Fayzullin *et al.*[8] added 0.25% antioxidant 1010 to PP/wood flour/glass bead composites and, after boiling water and room-temperature immersion tests as well as multiple extrusions, found that it significantly improved the modulus retention rate while reducing water absorption, melt index increment, and color difference. The mechanism involves 1010 preferentially providing hydrogen atoms to free radicals to terminate oxidation chains, thereby inhibiting interfacial deterioration. Khantimirov *et al.*[9] introduced a 1 : 1 composite of antioxidants 1010 and 168 into HDPE/wood flour composites, resulting in a 200% prolongation of oxidation induction time, a 55% reduction in the growth rate of the thermal aging carbonyl index, and a 98% tensile strength retention rate after five extrusions. The two components achieve enhancements in processing stability, long-term weatherability, and mechanical lifespan through synergistic chain termination and peroxide reduction. However, these studies primarily focus on non-degradable polyolefin matrices, with limited research on the unique 'hydrolysis-oxidation' coupled failure mechanism in polyester materials (*e.g.*, PLA) under humid-heat environments. Traditional antioxidant systems struggle to simultaneously capture free radicals and efficiently decompose hydroperoxides generated from ester bond hydrolysis, limiting the long-term service of fully biodegradable materials in complex environments.

To address these challenges, this work employs PLA as the matrix and *Salix psammophila* fibers as the reinforcing phase to construct a primary–secondary synergistic system of hydrothermal aging-resistant additives, systematically investigating its mechanism of action and performance evolution. The study analyzes the static and dynamic mechanical behaviors and molecular chain responses under hydrothermal aging, and develops a correlation model between static and dynamic properties; reveals interfacial damage paths through microscopic morphology; and elucidates chemical structure evolution and molecular chain scission behaviors. This research aims to clarify the aging mechanisms of the composites, providing supportive evidence based on statistical interpretation for improving their durability and structural optimization.

2 Experimental

2.1 Materials

Salix psammophila wood flour (SF, 40–60 mesh) was provided by Manlai Township, Ordos City, Inner Mongolia; polylactic acid (PLA, chemically pure) was purchased from Dongguan Zhanyang Polymer Materials Co., Ltd; maleic anhydride coupling agent (MAPP, analytically pure) was obtained from Nanjing Chuangshi Chemical Additives Co., Ltd; anhydrous ethanol (analytically pure) was sourced from Tianjin Fuyu Fine Chemical Co., Ltd; pentaerythritol tetrakis (1010, analytically pure) was acquired from Shandong Junrui Medical Technology Co., Ltd; distearyl thiodipropionate (DSTP, analytically pure) was purchased from Shanghai Yien Chemical Technology Co., Ltd These raw materials were used as received.

2.2 Preparation of *Salix psammophila*/polylactic acid composites

Maleic anhydride coupling agent amounting to 2% of the *Salix psammophila* wood flour mass was weighed. A 95% ethanol solution was prepared at a ratio of M(coupling agent): M(95% ethanol solution) = 1 : 5 and heated with stirring for 10 min at 80 °C using a magnetic stirrer to obtain the maleic anhydride coupling agent ethanol solution. The solution was evenly sprayed onto the *Salix psammophila* wood flour using a spray bottle for surface modification. The modified wood flour was dried in an oven at 70 °C until the moisture content was below 2%.

According to the experimental design, a two-step mixing process was employed. The weighed modified *Salix psammophila* wood flour, PLA, polyethylene wax, and hydrothermal aging-resistant additives were added in different proportions using a stepwise addition method. First, 30% of the materials were added to a high-speed mixer and mixed uniformly for 4 min, followed by the addition of the remaining 70% and mixing for another 6 min. The mixture was then evenly spread in a custom mold and pre-pressed for 10 min. Tin foil was used as an isolation layer to prevent adhesion between the material and the backing plate, facilitate demolding, protect the mold surface, and promote uniform heat distribution, ensuring consistent heating throughout the material and improving product quality.

After pre-pressing, the composites were hot-pressed in an experimental hot press to form *Salix psammophila*/polylactic acid composites. Based on preliminary process studies, the hot-pressing parameters were set as follows: temperature of 190 °C, time of 7 min, pressure of 7 MPa, *Salix psammophila* wood flour mesh size of 40–60, wood-to-polymer ratio of 3 : 7, maleic anhydride coupling agent addition of 2%, composite design density of 1.0 g cm^{-3}, and dimensions of 200 mm × 200 mm × 4 mm. The preparation process of the composites is illustrated in Fig. 1.

Blank samples without hydrothermal aging-resistant additives (WPC), samples with only 1.5 wt% 1010 (WPC-1010), and samples with 1.5 wt% 1010 and 1 wt% DSTP (WPC-1/D) were prepared as the main research objects. The compositions of each group are shown in Table 1.

2.3 Measurements

In accordance with the national standard GB/T 12 000–2017 "Plastics–determination of the effects of exposure to damp heat, water spray and salt mist", the hydrothermal aging temperature was set to 60 °C, with hydrothermal aging cycles of 0, 24, 48, 96, 144, and 168 h, respectively. After each cycle, the samples were removed, dried, and tested. The sample size was 50 mm × 50 mm × 4 mm.

The flexural strength MOR and elastic modulus MOE of the composites were determined according to the national standard GB/T 17 657–2022 "Test methods of evaluating the properties of

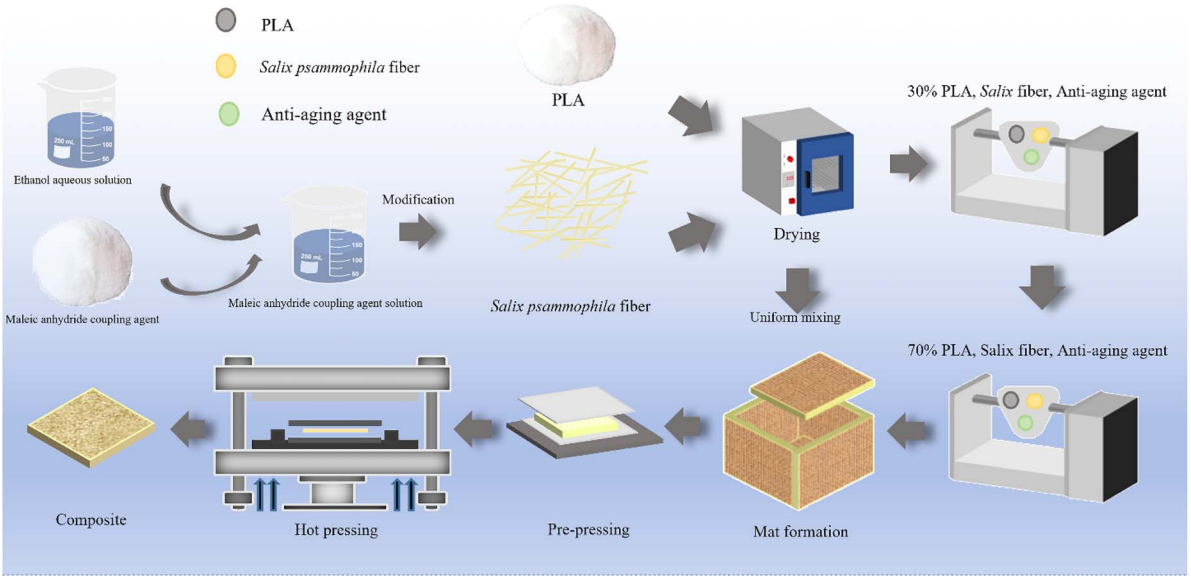

Fig. 1 The fabrication of *Salix psammophila*/polylactic acid composites.

Table 1 Composition ratios of composites with different additives

Num.	Sample name	SF/%	PLA/%	MAPP/%	PE/%	1010/wt%	DSTP/wt%
1	WPC	30	70	2	1.0	0	0
2	WPC-1010	30	70	2	1.0	1.5	0
3	WPC-1/D	30	70	2	1.0	1.5	1

wood-based panels and surface decorated wood-based panels", obtaining stress–strain curves under static mechanical properties, with all test temperatures at room temperature. The specimen dimensions were length $l = 150$ mm, width $b = 50$ mm, thickness $h = 4$ mm, the distance between the two supports was 100 mm, and the loading speed during the test was 20 mm min^{-1}.

The storage modulus E', loss modulus E'', and loss factor tan δ of the composites were tested using a dynamic thermo-mechanical analyzer DMA in accordance with the national standard GB/T 40 396–2021 "Test method for glass transition temperature of polymer matrix composites–dynamic mechanical analysis (DMA)". A three-point bending fixture and Multi-Frequency-Strain mode were adopted, with a test temperature range of −20 °C to 150 °C, heating rate of 5 °C min^{-1}, frequency of 1 Hz, amplitude of 25 μm, and Poisson's ratio of 0.44. The specimen dimensions were length $l = 55$ mm, width $b = 10$ mm, thickness $h = 4$ mm.

The surface, fracture surface morphology, and microstructure of the composites after hydrothermal aging at different stages were observed using a scanning electron microscope (JSM-6701F, purchased from JEOL Ltd, Japan). Before scanning, the composite surfaces and fracture surfaces were gold-sputtered, with a test voltage of 10 kV.

The functional groups of the composites were tested using a Fourier transform infrared spectrometer (TENSOR 27, purchased from Bruker, Germany). The measurement range was 4000–650 cm^{-1}, with a resolution of 4 cm^{-1}, and 32 scans.

XPS elemental analysis was performed on samples during the hydrothermal aging process (K-Alpha, purchased from Thermo Fisher Scientific), and the elemental valence states on the sample surface and interior were analyzed simultaneously.

Gel permeation chromatography GPC (Waters 1515–2414, purchased from Guangzhou Xiaofen Instrument Co., Ltd) was adopted to test the molecular weight size and distribution of PLA before and after degradation of the samples. Chromatographically pure THF was used as the mobile phase, with a flow rate of 1.0 mL min^{-1}, and column temperature of 35 °C. Before testing, the samples were dissolved in THF at a concentration of 5 mg mL^{-1}, filtered using a 0.22 μm polytetrafluoroethylene PTFE membrane, and then sampled. Calibration was performed using narrow-distribution polystyrene (PS) standards.

3 Results and discussion

3.1 Analysis of static mechanical properties of the composites

The static mechanical properties are shown in Fig. 2a. Before aging, the bending strengths of WPC-1010 and WPC-1/D were 27.13 MPa and 29.57 MPa, respectively, representing increases of 6.31% and 15.87% compared to WPC. After aging, the bending strengths of WPC-1010 and WPC-1/D were 11.77 MPa and 14.01 MPa, respectively, showing substantial improvements

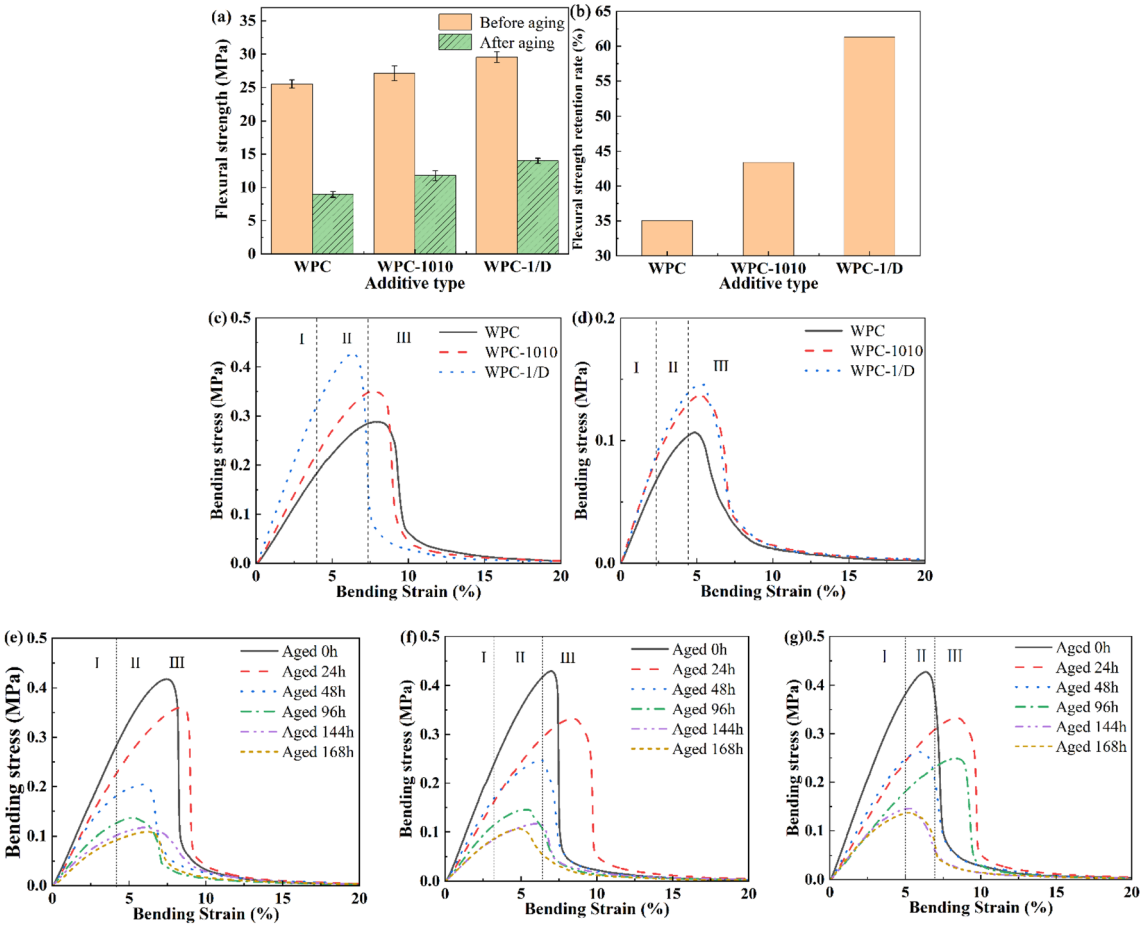

Fig. 2 Static mechanical properties and stress–strain behavior of SF/PLA composites with different additives: (a) flexural strength and (b) retention rate; comparative stress–strain curves (c) before and (d) after hydrothermal aging; and time-dependent stress–strain evolution for (e) WPC, (f) WPC-1010, and (g) WPC-1/D.

of 31.51% and 56.54% compared to WPC (8.95 MPa). As shown in Fig. 2b, the mechanical property retention rates were 43.38% and 47.38%, respectively, which were 8.31% and 12.31% higher than that of WPC (35.07%).

The enhanced performance of WPC-1/D benefits from the synergistic effects of 1010 and DSTP—1010 as the primary antioxidant captures free radicals, while DSTP decomposes hydroperoxides to reduce free radical generation. This dual mechanism effectively delays the degradation of the PLA matrix.[10] Similar reinforcement mechanisms have been reported in graphene-based sandwich structures, where a stiff interlayer can carry and redistribute axial loads, leading to a several-fold increase in both Young's modulus and fracture toughness.[11] Compared to WPC-1010, which improves compatibility and captures free radicals solely through hydrogen bonding of 1010, the primary-secondary synergistic system demonstrates a significantly greater enhancement in elastic modulus than the addition of a single additive.

The bending stress–strain behavior further confirms the static mechanical property test results: the failure process of the composites under static bending loads can be divided into three typical stages. As shown in Fig. 2c and d, in the first linear elastic stage (I), the curve slopes for WPC, WPC-1010, and WPC-1/D increase sequentially, with the matrix undergoing elastic deformation and the elastic modulus gradually increasing.[12] In the second non-linear elastic stage (II), before aging, the peak shape of WPC-1/D is sharper than those of WPC-1010 and WPC, exhibiting brittle characteristics but overall tending toward toughness; after aging, all materials shift toward brittleness, with WPC-1/D maintaining the relatively best peak shape. In the third damage accumulation and failure stage (III), after aging, the curves for WPC and WPC-1010 decline more slowly, showing certain tough fracture characteristics, while WPC-1/D declines faster, exhibiting a brittle fracture mode, which is consistent with the failure mechanisms of fiber-matrix interfacial debonding and fiber fracture.[13]

The stress–strain curves shown in Fig. 2e–g systematically reveal the deformation and failure behaviors of the three samples throughout the entire aging cycle (0–168 h). In the linear elastic stage (I), as aging time prolongs, the curve slope gradually decreases, and the elastic modulus continuously declines, with WPC showing the most significant modulus attenuation: rapid softening due to interfacial debonding in the early stage (0–48 h), a slowed decline rate but severe modulus

loss in the middle stage (48–144 h), and almost complete loss of rigidity in the late stage (144–168 h); WPC-1010 exhibits a more gradual modulus decline due to the antioxidative effect of 1010, but insufficient interfacial protection still leads to continuous deterioration; WPC-1/D maintains the optimal modulus in each aging stage owing to the synergistic effects of 1010 and DSTP, with the best preservation of interfacial bonding strength and matrix integrity. In the non-linear elastic stage (II), WPC rapidly loses its yield plateau as aging progresses, presenting typical brittle fracture characteristics; WPC-1010 maintains a shorter yield plateau but with limited plastic development; while WPC-1/D consistently shows a pronounced and extended yield plateau, with coordinated interfacial slip and matrix plastic deformation, retaining excellent toughness characteristics even in the late aging stage. In the damage accumulation and fracture failure stage (III), the stress curve of WPC exhibits an abrupt drop mode, with the weakest energy absorption capacity; WPC-1010 shows a slightly slower stress decline, but with limited toughness improvement; WPC-1/D displays the optimal fracture behavior, with gradual stress decline, impeded crack propagation, and significant fracture energy absorption, as the residual interfacial bonding force and matrix extensibility collectively delay material failure. The entire curve evolution process fully demonstrates that the primary-secondary synergistic system significantly enhances the deformation coordination and fracture toughness of the composites under long-term hydrothermal aging through multiple mechanisms of suppressing interfacial debonding, maintaining matrix plasticity, and delaying crack propagation.

3.2 Analysis of dynamic mechanical properties of composites

Analysis of the storage moduli (E') of the three comparative materials is shown in Fig. 3a. In the glassy state stage (I), the E' of WPC was only 697.11 MPa, while those of WPC-1010 and WPC-1/D containing additives were increased to 1262.33 MPa and 1295.43 MPa, respectively, with WPC-1/D achieving a synergistic enhancement effect through hydrogen bonding of 1010 and steric hindrance of DSTP, leading to denser molecular chain packing.[14] In the glass transition stage (II), E' decreased rapidly for all materials, but the decline rates for WPC-1010 and WPC-1/D were significantly slower than that for the blank sample, indicating that the additives effectively delayed chain segment motion and the glass transition process. In the rubbery state stage (III), WPC-1/D still maintained the highest E' value, exhibiting the best interfacial stability and rigidity retention capability, while WPC had the lowest E', illustrating that the additives markedly enhanced the structural stability of the material in the rubbery state by restricting PLA molecular chain motion and reducing free volume.[15]

As shown in Fig. 3b and c, analysis of the loss modulus (E'') and loss factor (tan δ) indicates that in the glassy state region (I), WPC-1/D achieved the highest E'' and tan δ due to enhanced molecular chain interactions from the primary–secondary synergistic system, demonstrating that the additives synchronously improved viscous dissipation and internal friction performance through increased interfacial friction and interchain forces.[16] WPC-1010 showed increased values for both

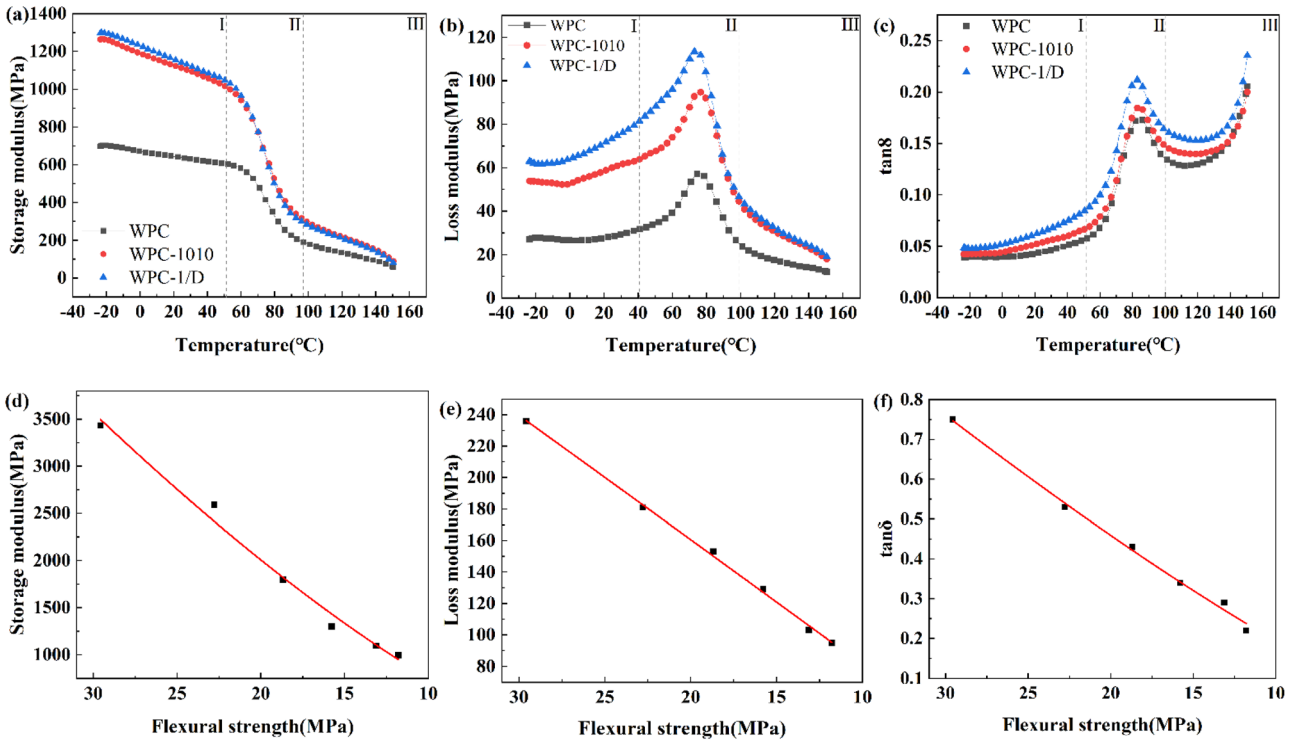

Fig. 3 Dynamic mechanical properties and their correlation with static strength for SF/PLA composites: (a) storage modulus, (b) loss modulus, and (c) loss factor for different additive types; and non-linear fitting curves of MOR *versus* (d) E', (e) E'', and (f) tan δ at 60 °C.

due to enhanced interfacial friction introduced by 1010, while WPC had the lowest E'' and tan δ. In the glass transition region (II), E'' and tan δ reached peaks simultaneously, with the T_g of WPC-1010 increased to 86.60 °C and a significant increase in E'', confirming that 1010 effectively suppressed molecular chain motion; WPC-1/D exhibited the highest E'' peak and tan δ peak (corresponding to $T_g = 84.18$ °C), as the hydrogen bonding of 1010 and steric hindrance of DSTP synergistically enhanced chain segment friction and interfacial bonding, optimizing energy dissipation capacity. Upon entering the rubbery state (III), E'' gradually decreased, while tan δ showed a trend of first decreasing and then increasing; WPC-1/D consistently maintained the highest E'' and tan δ values, indicating that it could still sustain excellent energy dissipation capacity in the rubbery state through continuous interfacial friction and restricted molecular chain motion. Overall, the primary–secondary synergistic system significantly enhanced the damping performance and interfacial stability of the material across all stages by regulating viscoelastic responses.

Correlation analysis was performed on the static and dynamic mechanical property data of WPC-1/D after hydrothermal aging at 60 °C for different times (0–168 h), with nonlinear fitting of static-dynamic properties. Flexural strength reflects the macroscopic overall mechanical behavior, while dynamic mechanical properties (including storage modulus E', loss modulus E'', and loss factor tan δ) reveal microscopic molecular chain motion and thermal transition behaviors; their combination allows for a deeper understanding of aging mechanisms and performance evolution laws.

The non-linear fitting results indicate a highly significant power-law relationship between flexural strength and each dynamic mechanical parameter (E', E'', tan δ), with correlation coefficients R^2 of all fitting equations exceeding 0.98. The fitting curves are shown in Fig. 3d–f, and specific parameters are listed in Table 2. This high correlation implies that performance in one aspect can be effectively predicted using data from a single static or dynamic property.

The study indicates that the correlation between static and dynamic mechanical properties exhibits significant temperature dependence: during high-temperature aging at 60 °C, the response of dynamic parameters to MOR becomes more gradual (with an increase in a value and a decrease in b value), suggesting that elevated temperatures accelerate molecular chain scission and weaken the property associations; meanwhile, the b value for tan δ and MOR remains stable at 1.21–1.25, confirming a stable non-linear positive correlation between the material's damping performance and static strength. The model parameters a and b can serve as effective indicators for quantifying interface bonding strength and molecular chain mobility. By setting a failure threshold of $E' = 1000$ MPa, the critical lifespan under aging at 40 °C can be predicted to be approximately 200 h (with a recommendation for replacement before 150 hours), and this approach can guide adjustments to composition and processes to reduce R&D costs and accelerate material optimization.

3.3 Analysis of microscopic morphology of composites

Fig. 4 shows the comparison of microscopic morphologies of the three composites after aging. Before aging, the resin matrix surfaces of all samples were relatively smooth without significant defects; after aging, the surface of WPC (d) was the roughest, exhibiting numerous cracks, pits, pores, and wood flour exposure, covered with PLA hydrolysis crystalline powder, indicating severe degradation.[17] The surface of WPC-1010 (*f*) was relatively rough, with a small number of defects and less wood flour exposure; the surface particles were co-crystals of PLA and 1010.[18] WPC-1/D (*h*) performed the best, with the surface only slightly rough, exhibiting very few defects and trace wood flour exposure; the surface was the whitest, and its particles were co-crystals of PLA, 1010, and DSTP. The damage paths of the three showed fundamental differences: WPC followed a failure path from surface crack initiation, intensified interfacial debonding, internal crack propagation to overall delamination; WPC-1010 had fewer surface cracks, milder interfacial debonding, slower internal crack propagation, and better overall structural integrity; while the WPC-1/D system significantly delayed this process, greatly suppressing surface cracks, interfacial debonding, and internal crack propagation, maintaining good overall structure.

The fracture morphologies of the materials before and after aging were observed and analyzed using scanning electron microscopy. As shown in Fig. 5, before aging, all samples (a) exhibited good interfacial bonding, but differences in fracture characteristics: WPC (b) was brittle with some toughness fracture, with more fiber pull-out and smaller voids; WPC-1010 (c) showed ductile fracture with less fiber pull-out; WPC-1/D (d) had the most pronounced toughness characteristics, with the least fiber pull-out and fracture, and the smallest voids, indicating its optimal initial interfacial bonding. After aging, WPC transitioned to brittle fracture, with obvious interfacial debonding, extensive fiber pull-out, and enlarged voids; while WPC-1010 and WPC-1/D retained mixed brittle-tough characteristics, with slight interfacial debonding, among which WPC-1/D performed the best, with the least fiber pull-out, the smallest voids, and the highest interfacial strength. This

Table 2 Fitting equations for static mechanical properties (x) and dynamic mechanical properties (y)

Aging temperature	Performance indicator	Fitting formula	a	b	R^2
60 °C	E'	$y = a \times x^b$	48.90674	1.25421	0.98632
	E''		6.07277	1.0818	0.99503
	Tan δ		0.0123	1.21123	0.98683

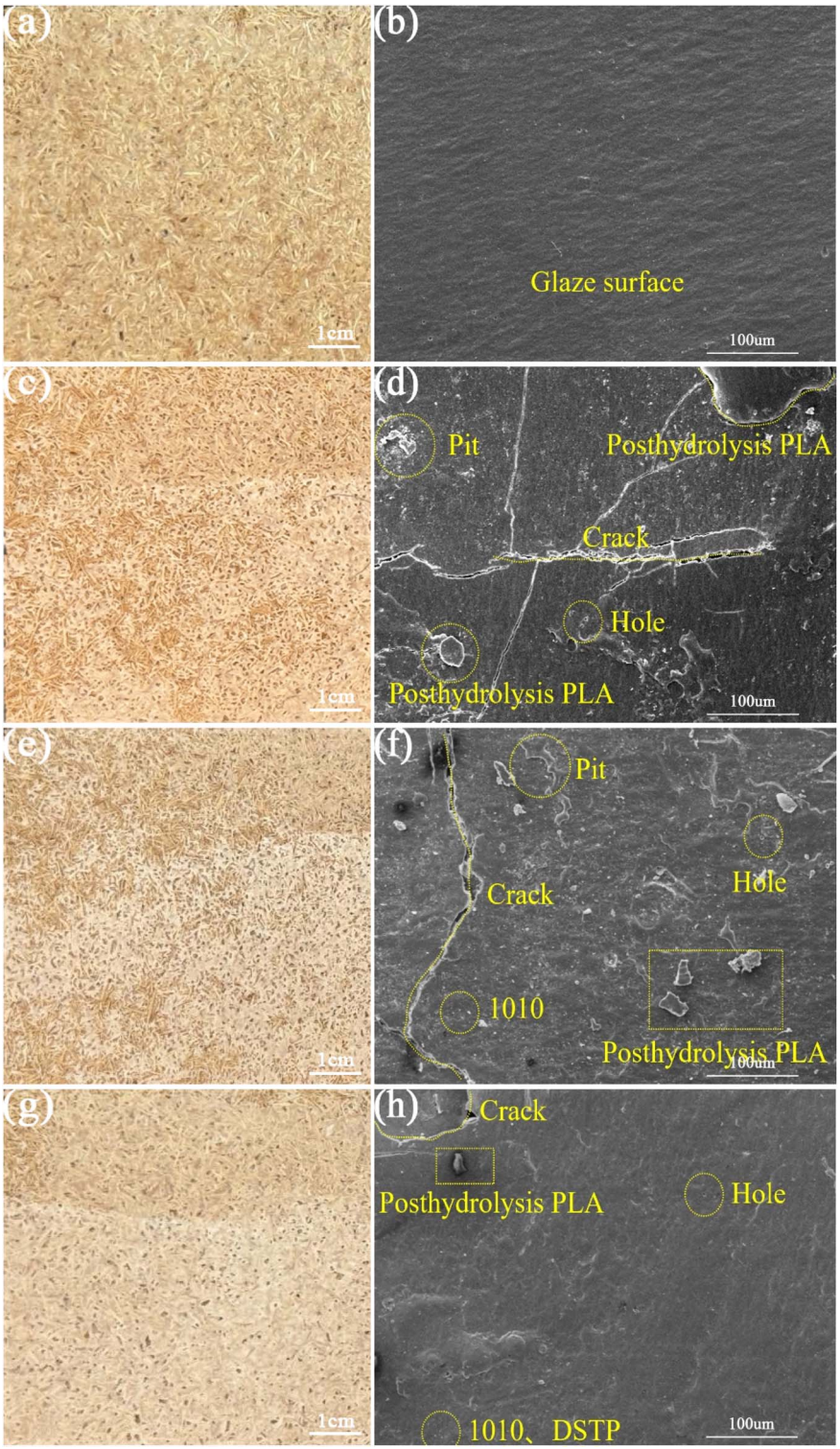

Fig. 4 Apparent and microscopic surface morphologies of SF/PLA composites: (a and b) before aging; and after hydrothermal aging for (c and d) WPC, (e and f) WPC-1010, and (g and h) WPC-1/D.

indicates that 1010 effectively delayed aging, while the 1010/DSTP synergistic system more significantly inhibited crack propagation and interfacial debonding, transforming the material failure path from "surface—interface—interior—overall" complete destruction to a slow accumulation of damage.

Combining macro-micro morphologies, mechanical properties, and chemical degradation analysis, the damage evolution of the composites during hydrothermal aging can be divided into three stages, with failure modes in each stage closely related to the material matrix and interfacial chemical

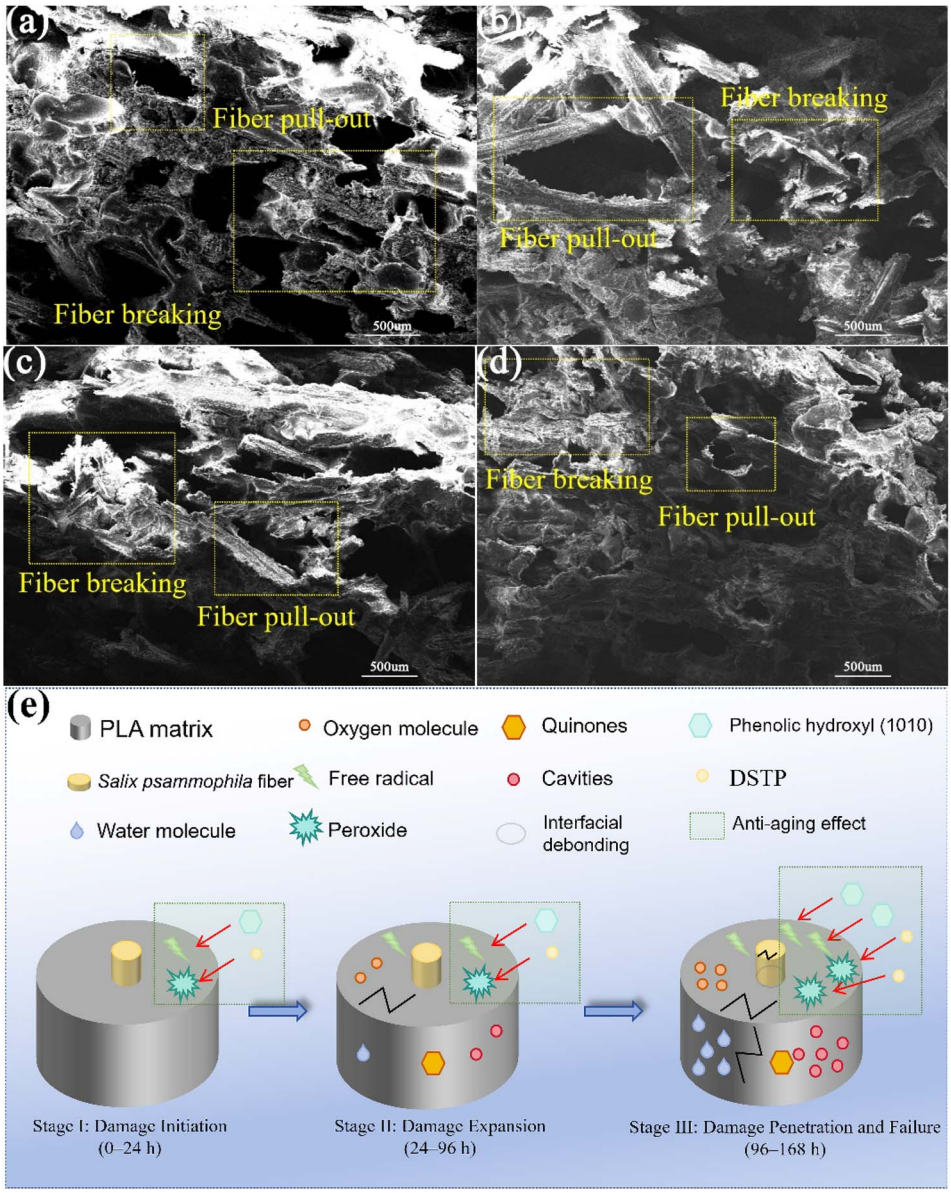

Fig. 5 The SEM images of: (a) initial fracture surface; (b–d) fracture surfaces after hydrothermal aging for (b) WPC, (c) WPC-1010, and (d) WPC-1/D; and (e) schematic illustration of the damage evolution process and failure modes.

changes. The corresponding damage evolution process and failure modes are shown in Fig. 5e.

In the initial damage initiation stage (Stage I, 0–24 h), The surface of the material was smooth and intact, with no visible cracks. PLA ester bonds undergo only slight hydrolysis, generating a small amount of carboxylic acids and initial free radicals,[19] but the hydrothermal aging primary agent 1010 can effectively capture these free radicals, and the auxiliary agent DSTP timely decomposes peroxides, thereby delaying the oxidative degradation process. Although localized stress concentration leads to microcrack initiation in the matrix, it has not yet extended to the interfacial region.

In the micro-damage expansion stage (Stage II, 24–96 h), obvious defects such as microcracks and pits begin to appear on the material surface. Some *Salix psammophila* wood flour starts to be exposed. At this time, the PLA hydrolysis reaction accelerates, with significant autocatalytic effect of carboxylic acids,[20] and lignin oxidation generates quinone substances. The difference between matrix shrinkage and fiber expansion leads to increased interfacial stress, causing partial debonding, and the matrix strength has obviously decreased.

In the damage penetration and failure stage (Stage III, 96–168 h), it manifests as extension and connection of surface cracks and obvious delamination. The PLA matrix is severely degraded, with large areas of pores, *Salix psammophila* wood flour completely exposed and fractured, and complete interfacial bonding failure. At this time, a large number of PLA ester bonds break, *Salix psammophila* wood flour deeply oxidizes, and the additives are exhausted, leading to uncontrolled synergistic effects of oxidation-hydrolysis. Interfacial debonding and

matrix cracks interconnect, fibers bear load alone and then fracture, with extensive fiber pull-out traces visible on the fracture surface.

In the destruction process from damage initiation to damage expansion to damage penetration, the primary–secondary synergistic system can significantly improve the durability of the composites through the dual mechanisms of free radical capture and hydroperoxide decomposition. This provides important empirical insights for developing high-performance bio-based composites.

3.4 FTIR analysis of composites

The Fourier transform infrared spectra (FT-IR) of the three materials are shown in Fig. 6a. WPC exhibits typical degradation characteristics, with the O–H stretching vibration peak blue-shifted from 3384 cm^{-1} to 3422 cm^{-1}, indicating hydrogen bond destruction and free hydroxyl group formation; the ester group C=O peak shifted from 1756 cm^{-1} to 1758 cm^{-1}, confirming ester bond hydrolysis to generate carboxylic acid; a new secondary alcohol C–O peak at 1133 cm^{-1}, and enhanced $-CH_3$ and $-CH_2$- peaks at 3000 cm^{-1} and 2946 cm^{-1}, collectively indicating PLA main chain scission and generation of oxidation byproducts; meanwhile, the blue shift of the cellulose C–O peak at 1087 cm^{-1} (to 1089 cm^{-1}) reflects hydrolysis of the wood flour components. For WPC-1010, due to the addition of 1010, the shift of the O–H peak from 3334 cm^{-1} to 3426 cm^{-1} is reduced, and the $-CH_3$ peak is only weakly enhanced, showing that it effectively inhibits oxidation reactions by capturing free radicals, but has limited protective effect on ester bond hydrolysis, as evidenced by the C=O peak at 1748 cm^{-1} still shifting to 1758 cm^{-1}. WPC-1/D exhibits the best stability, with the O–H peak changing most gradually from 3332 cm^{-1} to 3422 cm^{-1}, the ester group C=O only slightly displaced, no new $-CH_3$ peak, and the C–O peak at 1082 cm^{-1} remaining stable; these features confirm that the synergistic action of 1010 and DSTP can simultaneously inhibit oxidation and hydrolysis—1010 blocks oxidation chain reactions by clearing free radicals, while DSTP protects ester bonds and fiber-matrix interface by decomposing peroxides.

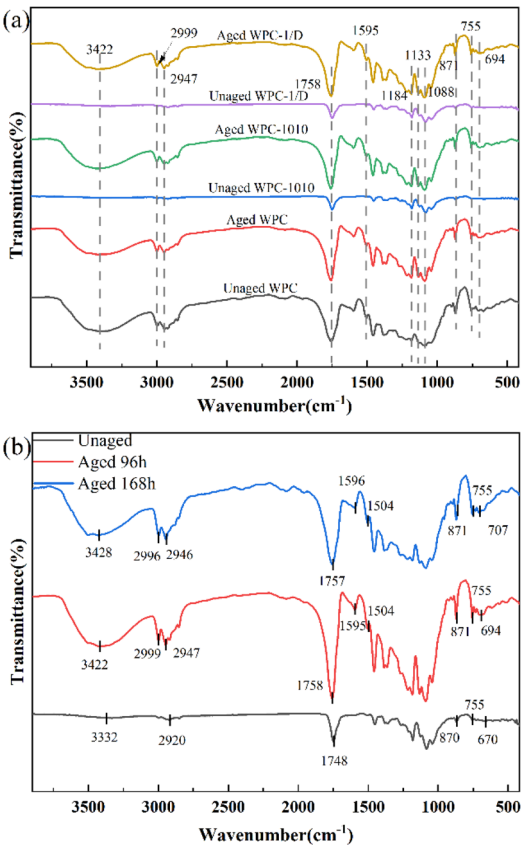

Fig. 6 FTIR spectra of SF/PLA composites: (a) comparative analysis of different additive types after hydrothermal aging; and (b) time-dependent spectral evolution of the WPC-1/D specimen from 0 to 168 h.

Analysis of the Fourier transform infrared functional spectra of WPC-1/D over 168 hours (Fig. 6b) shows that in the C–H bond region, the characteristic peak initially at 2920 cm^{-1} gradually shifts to 2947 cm^{-1} (96 h) and a weak $-CH_3$ peak appears at 2999 cm^{-1}, indicating limited scission of local chain segments, but by 168 h, the peak intensities at 2996 cm^{-1} and 2946 cm^{-1} do not further significantly enhance, confirming that the primary–secondary synergistic system continuously inhibits PLA main chain scission; in the O–H bond region, the hydrogen-bonded peak at 3332 cm^{-1} gradually blue-shifts to 3422 cm^{-1} (96 h) and 3428 cm^{-1} (168 h), this progressive change amplitude is significantly smaller than the system without additives, indicating that 1010 effectively delays hydroxyl oxidation by capturing free radicals; in the ester group region, the C=O characteristic peak at 1748 cm^{-1} only blue-shifts 10 cm^{-1} to 1758 cm^{-1} after 96 h with stable peak intensity, remaining at 1757 cm^{-1} by 168 h, proving that DSTP effectively protects ester bond integrity by decomposing peroxides; additionally, the lignin characteristic peaks at 1595–1596 cm^{-1} and 1504 cm^{-1}, and the aromatic ring C–H vibrations in the fingerprint region at 870 cm^{-1}, 755 cm^{-1}, 707 cm^{-1} remain stable throughout the aging process, indicating that the lignin structure in *Salix psammophila* wood flour is not significantly damaged.[21] These results collectively confirm that the primary–secondary synergistic system effectively maintains the structural stability of the composites during long-term aging through the antioxidative action of 1010 and the anti-hydrolytic action of DSTP.

3.5 XPS analysis of composites

X-ray photoelectron spectroscopy (XPS) analysis revealed distinct elemental compositions and chemical bond changes in the three samples after 96 hours of hydrothermal aging. For WPC (Fig. 7a and b), the carbon content decreased from 76.29% to 74.19%, while the oxygen content increased from 22.72% to 24.80%. The C–C/C–H bond content reduced from 69.09% to 50.33%, the C=C bond content sharply decreased from 20.16% to 4.85%, the C=O bond content increased from 9.7% to 15.9%, and the C–O bond content dramatically rose from 1.05% to 28.91%. These changes, combined with the corresponding peak shifts in FTIR (O–H peak from 3384 to 3422 cm^{-1}, C=O peak

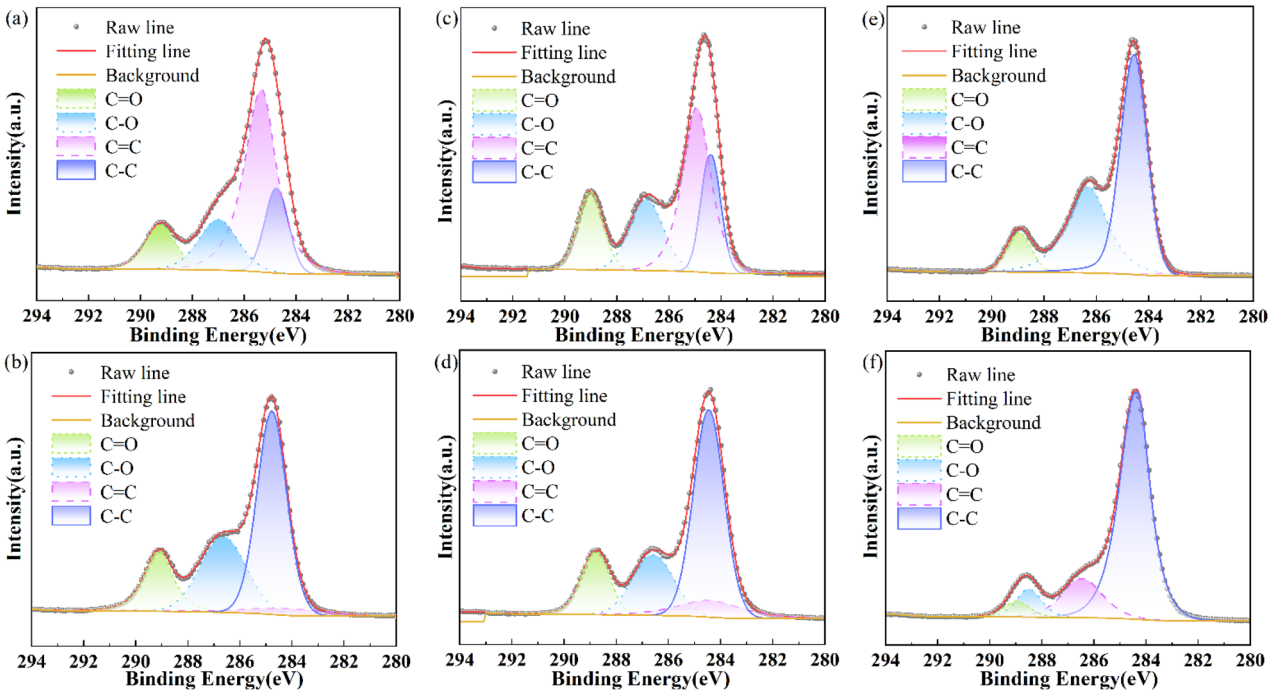

Fig. 7 XPS C 1s peak-fitting spectra of SF/PLA composites before and after hydrothermal aging: (a and b) WPC, (c and d) WPC-1010, and (e and f) WPC-1/D.

from 1756 to 1758 cm^{-1}, and a new secondary alcohol C–O peak at 1133 cm^{-1}), collectively confirm the synergistic degradation mechanism involving PLA main chain scission, ester bond hydrolysis, and lignin oxidation.[22]

For WPC-1010 (Fig. 7c and d), the carbon content increased from 71.47% to 75.17%, the oxygen content decreased from 28.35% to 23.71%, the C–C/C–H bond content increased to 53.79%, and the nitrogen content rose from 0.01% to 1.00%. Combined with the smaller O–H peak shift in FTIR (from 3334 to 3426 cm^{-1}) and C=O peak shift (from 1748 to 1758 cm^{-1}), this indicates that 1010 effectively inhibited oxidation reactions by capturing free radicals, but its protective effect against ester bond hydrolysis was limited.

WPC-1/D (Fig. 7e and f) exhibited the optimal surface chemical stability, with the carbon content substantially increasing from 73.88% to 80.03%, the oxygen content significantly decreasing from 25.92% to 18.80%, the C–C/C–H bond content markedly increasing to 72.84%, and the C=O bond content decreasing to 7.16%. Notably, the nitrogen content was extensively introduced, surging from 0.02% to 4.67%, and the sulfur content increased from 0.20% to 0.96%, verifying that 1010 as the primary antioxidant cleared free radicals to inhibit oxidation, while DSTP as the auxiliary antioxidant decomposed peroxides to inhibit hydrolysis, achieving the optimal surface chemical stability.

3.6 GPC analysis of composites

The gel permeation chromatography (GPC) spectra of the three materials are shown in Fig. 8, with relative molecular weights listed in Table 3.

For WPC, the number-average molecular weight (M_n), weight-average molecular weight (M_w), and peak molecular weight (M_p) increased by 15.48%, 10.99%, and 29.21%, respectively, while the polydispersity index (PDI) decreased by 3.89%; the peak broadened and elution occurred earlier. This apparent molecular weight increase results from preferential degradation of low-molecular-weight components, combined with the FTIR ester C=O peak shift from 1756 cm^{-1} to 1758 cm^{-1} and XPS C–C bond content decrease from 69.09% to 50.33%, confirming PLA main chain scission under synergistic hydrolysis and oxidation.[23]

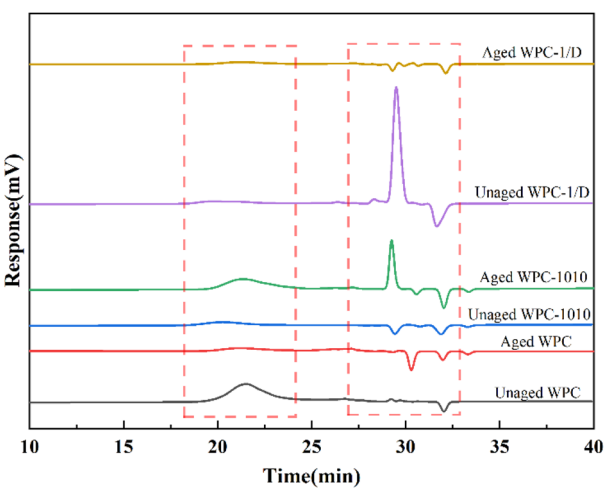

Fig. 8 GPC spectra for different additive types.

Table 3 Relative molecular weights for different additive types

	Before aging			After aging			Improvement rate		
	WPC	WPC-1010	WPC-1/D	WPC	WPC-1010	WPC-1/D	WPC	WPC-1010	WPC-1/D
Mn (g mol^{-1})	120 791	38 399	41 837	139 491	136 411	153 604	15.48%	255.24%	267.15%
Mw (g mol^{-1})	282 326	76 087	78 062	313 357	283 723	317 009	10.99%	272.89%	306.10%
Mp (g mol^{-1})	247 104	68 809	104 615	319 286	285 538	315 117	29.21%	314.97%	201.22%
PDI	2.3373	1.9814	1.8658	2.2464	2.0799	2.0638	−3.89%	4.97%	10.61%

The unexpected decrease in surface oxygen content indicates significant surface enrichment of hydrophobic additives (1010 and DSTP) during aging; the migration of these carbon-rich compounds may form a protective layer, masking the oxidation-degradation signals of the underlying PLA matrix. However, the molecular weight changes in WPC-1010 during aging are more pronounced, with M_n, M_w, and M_p increasing by 255.24%, 272.89%, and 314.97%, respectively, and PDI increasing by 4.97%; the peak distribution is narrower with delayed elution. Combined with the minor FTIR O–H peak shift (from 3334 to 3426 cm^{-1}) and XPS C–C bond content increase from 42.91% to 53.79%, this indicates that 1010 effectively inhibits molecular chain oxidative scission by capturing free radicals, although the significant molecular weight increase also suggests the occurrence of partial cross-linking reactions.[24]

WPC-1/D exhibits the optimal molecular weight retention characteristics, with M_n, M_w, and M_p increasing by 267.15%, 306.10%, and 201.22%, respectively, and PDI increasing by 10.61%; the peak distribution is the most concentrated with the latest elution. Combined with the minimal FTIR ester peak shift (from 1748 to 1758 cm^{-1}) and XPS C–C bond content marked increase from 55.19% to 72.84%, this confirms that the primary-secondary synergistic system effectively inhibits polymer main chain scission through the synergistic actions of 1010 clearing free radicals to suppress oxidation and DSTP decomposing peroxides to block hydrolysis, while maintaining the integrity of high-molecular-weight segments during selective degradation of low-molecular-weight components. Comprehensive analysis indicates that the molecular weight retention and distribution control capabilities of WPC-1/D are significantly enhanced to those of WPC and WPC-1010, demonstrating that the primary–secondary synergistic system enhances the molecular stability of the composites through dual protection mechanisms.

4 Conclusions

(1) The 1010/DSTP primary–secondary synergistic system significantly enhanced the anti-aging performance of the composites, with bending strength increased by 15.87% after aging, and flexural strength retention rate maintained above 47.4%. This system constructs a synergistic network through 1010 capturing free radicals and DSTP decomposing hydroperoxides, effectively suppressing PLA matrix hydrolysis and fiber-matrix interfacial damage.

(2) Dynamic mechanical analysis indicates that the synergistic system significantly delayed the performance decay of the composites under hydrothermal aging at 60 °C, effectively maintaining the stability of storage modulus and loss factor. The static-dynamic mechanical correlation model (R^2 > 0.98) constructed based on experimental data demonstrates a strong empirical relationship, providing supportive evidence based on a statistical interpretation for material lifespan assessment and process optimization.

(3) Microscopic morphology revealed three stages of material damage evolution: microcrack initiation (0–24 h), interface debonding expansion (24–96 h), and macroscopic delamination penetration (96–168 h). The synergistic system, relying on dual anti-aging mechanisms, significantly delayed the formation and expansion processes of the aforementioned microscopic damages.

(4) FTIR, XPS, and GPC characterizations confirmed that the system, through inhibiting oxidation reactions and blocking hydrolysis paths, effectively delayed PLA ester bond hydrolysis and lignin oxidative degradation. This dual protection mechanism significantly enhanced the chemical stability of the composites, providing a solid theoretical basis for achieving long-term durability of the materials.

Conflicts of interest

There are no conflicts of interest to declare.

Data availability

The data supporting the findings of this study are available within the article.

Acknowledgements

This work was financially supported by the General Project of Inner Mongolia Natural Science Foundation (No. 2024LHMS03020), and the Program for improving the Scientific Reasearch Ability of Youth Teachers of Inner Mongolia Agricultural University (No. BR220124).

Notes and references

1 S. H. Kamarudin, M. S. Mohd Basri, M. Rayung, *et al.*, A review on natural fiber reinforced polymer composites (NFRPC) for sustainable industrial applications, *Polymers*, 2022, **14**, 3698.

2 V. Prasad, A. Alliyankal Vijayakumar, T. Jose, *et al.*, A comprehensive review of sustainability in natural-fiber-reinforced polymers, *Sustainability*, 2024, **16**, 1223.
3 P. Baker, A. Charlton, C. Johnston, *et al.*, A review of Willow (Salix spp.) as an integrated biorefinery feedstock, *Ind. Crops Prod.*, 2022, **189**, 115823.
4 R. Wang, Z. Meng and Y. Gao, Chemical characteristics of *Salix psammophila* sand barriers are accelerated degradation by ultraviolet irradiation and water, *Front. Plant Sci.*, 2024, **15**, 1470347.
5 B. Anda, P. Oskars, J. V. Jana, *et al.*, Analysis of bio-based acrylate accelerated weathering: A study of nanocellulose impact on the bulk durability of 3D-printed nanocomposites, *Mater. Today Chem.*, 2023, **33**, 101683.
6 P. S. Shin, J. H. Kim, H. S. Park, *et al.*, A review: mechanical and interfacial properties of composites after diverse types of aging using micromechanical evaluation, *Fibers Polym.*, 2020, **21**, 225.
7 K. Arunprasath, P. Senthamaraikannan, I. Suyambulingam, *et al.*, From Degradation to Durability: Strategies for Prolonging the Shelf Life of Natural Fiber Composites–A Comprehensive Review, *J. Nat. Fibers*, 2025, **22**, 2554897.
8 I. Z. Fayzullin, I. N. Musin, S. I. Volfson, *et al.*, Glass-Filled Wood-Polymer Composites Based on Polypropylene, *Key Eng. Mater.*, 2019, **816**, 197.
9 A. G. Khantimirov, L. A. Abdrakhmanova, R. K. Nizamov, *et al.*, Investigation of properties in nanomodified polyethylene-based wood-polymer composites, *Nanotechnol. Constr.*, 2023, **15**, 110.
10 Z. Khan, F. Javed, Z. Shamair, *et al.*, Current developments in esterification reaction: A review on process and parameters, *J. Ind. Eng. Chem.*, 2021, **103**, 80.
11 B. Shin, Y. Zhu, Q. Ai, *et al.*, Mechanical Toughening of Two-Dimensional Covalent Organic Frameworks Enabled by Graphene-Based Sandwich-Structured Nanocomposites, *ACS Mater. Lett.*, 2025, **8**, 130–136.
12 A. Dao, J. Shimokata, K. Takeuchi, *et al.*, Stabilization of recombinant spider silk in thermo-oxidative degradation: high-throughput screening for antioxidants, *Polym. Degrad. Stab.*, 2018, **153**, 37–46.
13 A. K. Bledzki and A. Jaszkiewicz, Mechanical performance of biocomposites based on PLA and PHBV reinforced with natural fibres–A comparative study to PP, Compos, *Sci. Technol.*, 2010, **70**, 1687.
14 R. Lach, G. H. Michler and W. Grellmann, Microstructure and Indentation Behaviour of Polyhedral Oligomeric Silsesquioxanes-Modified Thermoplastic Polyurethane Nanocomposites, *Macromol. Mater. Eng.*, 2010, **295**, 484.
15 V. H. Rolón-Garrido and M. H. Wagner, Linear and non-linear rheological characterization of photo-oxidative degraded LDPE, *Polym. Degrad. Stab.*, 2014, **99**, 136.
16 G. Molero, S. Du, M. Mamak, *et al.*, Experimental and numerical determination of adhesive strength in semi-rigid multi-layer polymeric systems, *Polym. Test.*, 2019, **75**, 85.
17 M. Assarar, D. Scida, A. El Mahi, *et al.*, Influence of water ageing on mechanical properties and damage events of two reinforced composite materials: Flax–fibres and glass–fibres, *Mater. Des.*, 2011, **32**, 788.
18 H. Tsuji, H. Takai, N. Fukuda, *et al.*, Non-isothermal crystallization behavior of poly (L-lactic acid) in the presence of various additives, *Macromol. Mater. Eng.*, 2006, **291**, 325.
19 J. Hallstein, E. Metzsch-Zilligen and R. Pfaendner, Long-term thermal stabilization of poly (lactic acid), *Materials*, 2024, **17**, 2761.
20 R. Hedthong, T. Kittikorn, P. Damsongsee, *et al.*, Investigation of physico-chemical degradation through weathering acceleration of hemp/PLA biocomposite: thermal analysis, *J. Therm. Anal. Calorim.*, 2023, **148**, 2685.
21 Y. Bouramdane, S. Fellak, F. El Mansouri, *et al.*, Impact of natural degradation on the aged lignocellulose fibers of Moroccan cedar softwood: structural elucidation by infrared spectroscopy (ATR-FTIR) and X-ray diffraction (XRD), *Fermentation*, 2022, **8**, 698.
22 H. Gan, Y. Enomoto, T. Kabe, *et al.*, Synthesis, properties and molecular conformation of paramylon ester derivatives, *Polym. Degrad. Stab.*, 2017, **145**, 142.
23 F. R. Beltrán, E. Climent-Pascual, M. U. de la Orden, *et al.*, Effect of solid-state polymerization on the structure and properties of mechanically recycled poly (lactic acid), *Polym. Degrad. Stab.*, 2020, **171**, 109045.
24 B. Rimez, G. Van Assche, S. Bourbigot, *et al.*, Modelled decomposition kinetics of flame retarded poly (vinyl acetate), *Polym. Degrad. Stab.*, 2016, **130**, 245.